Wester and Kessler review evidence supporting the promise of polyvalent αvβ3-integrin antagonists, such as peptide multimers and peptide-polymer conjugates, as ligands for use in radiotherapeutic targeting of integrins involved in angiogenesis. . . . . ***Page 1940***

Boswell and Brechbiel outline the rationale for the utility of a new class of trifunctional somatostatin analogs (described elsewhere in this issue) that are transported into both targeted tumor cells and into the nuclei, where Auger electrons are most lethal. . . . . ***Page 1946***

COLOR

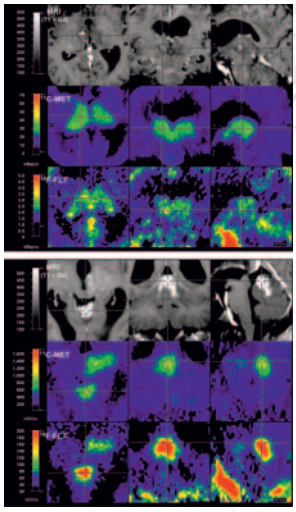

Jacobs and colleagues compare the diagnostic effectiveness of ^{18}F-fluoro-L-thymidine and ^{11}C-methylmethionine as markers of increased transport and proliferation in primary central nervous system tumors. . . . . ***Page 1948***

Lopresti and colleagues describe simplified methods for analysis of retention of the amyloid-binding Pittsburgh Compound in PET imaging in patients with Alzheimer's disease and in healthy individuals. . . . . ***Page 1959***

Yamauchi and colleagues use ^{11}C-flumazenil PET to measure benzodiazepine receptors to determine whether selective neuronal damage is associated with border-zone infarction in internal carotid artery occlusive disease. . . . . ***Page 1973***

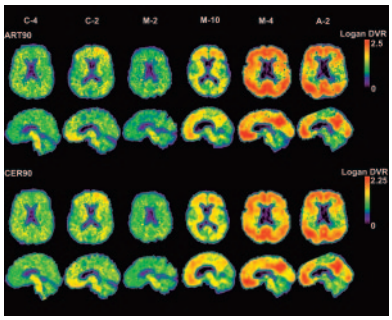

Costes and colleagues describe the binding potential of ^{18}F-MPPF, a novel serotonin 5-HT$_{1A}$ antagonist PET tracer with promise in serotoninergic system imaging, and discuss the importance of a robust normative database for additional research. . . . . ***Page 1980***

Heston and Sigg quantify the relative contributions of end-diastolic and end-systolic volumes to an optimized stress-induced volume ratio in patents undergoing gated SPECT imaging for myocardial ischemia. . . . . ***Page 1990***

Pellegrino and colleagues assess the relationship between brachial artery flow–mediated dilation and coronary flow reserve as estimated by sestamibi imaging in patients with peripheral artery disease. . . . . ***Page 1997***

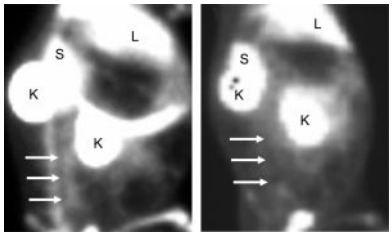

Elhendy and colleagues investigate whether stress ^{99m}Tc-tetrofosmin myocardial perfusion imaging can independently provide information for predicting mortality in patients with stable angina pectoris. . . . . ***Page 2003***

Khorsand and colleagues evaluate myocardial electrocardiography-gated ^{13}N-ammonia PET in the simultaneous assessment of myocardial perfusion, left ventricular geometry, and contractile function. . . . . ***Page 2009***

Bleeker-Rovers and colleagues assess the value of ^{18}F-FDG PET imaging in detecting metastatic infectious foci in patients with bacteremia or fungemia at high risk of metastatic infection. . . . . ***Page 2014***

Lejeune and colleagues use a decision analysis model to compare the cost effectiveness within the French health care system of CT with and without PET in the diagnosis and staging of patients with metachronous liver metastases of colorectal cancer. . . . . ***Page 2020***

COLOR

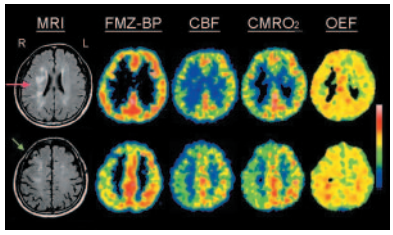

Wieder and colleagues evaluate chemotherapy-induced changes in tumor glucose use and tumor size in patients with adenocarcinoma of the esophagogastric junction undergoing ^{18}F-FDG PET and CT imaging before, during, and after neoadjuvant chemotherapy. . . . . ***Page 2029***

Boersma and colleagues review the clinical relevance, limitations, and potential applications of visualizing apoptosis with

the programmed cell–detecting protein annexin A5. . . . . ***Page 2035***

Hartung and colleagues explore the effects of dietary modification and statin therapy (measures known to favorably influence outcomes in coronary disease) on apoptosis in experimental atherosclerotic lesions. . . . . ***Page 2051***

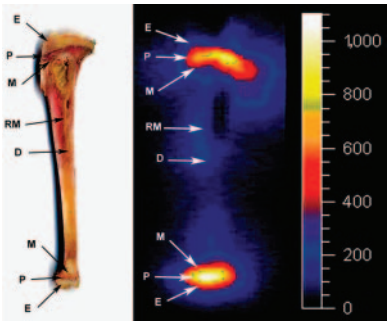

Verwijnen and colleagues compare the renal uptake effects of oral and intravenous administration of D-lysine in rats injected with ^{111}In- DTPA-octreotide, in an effort to surmount current limitations in tumor therapy with radiolabeled somatostatin analogs. . . . . ***Page 2057***

Bäck and colleagues investigate the relative biological effectiveness of the α-emitter ^{211}At and that of ^{60}Co γ-irradiation in a mouse radioimmunotherapy model of intraperitoneal ovarian cancer. . . . . ***Page 2061***

Buursma and colleagues evaluate the feasibility of monitoring gene therapy with the human norepinephrine transporter as a reporter gene in combination with the reporter probe ^{11}C-*m*-hydroxyephedrine in PET imaging. . . . . ***Page 2068***

Essman and colleagues determine the distribution of ^{153}Sm-EDTMP, a focus of interest in the treatment of primary osteosarcoma, within the tibias of juvenile rabbits and estimate the radiation-absorbed doses delivered to the physeal cartilage. . . . . ***Page 2076***

Brambilla and colleagues report the results of performance measurements for the lutetium oxyorthosilicate–based whole-body PET/CT scanner Biograph 16 HI-REZ using the National Electrical Manufacturers Association NU 2-2001 standard. . . . . ***Page 2083***

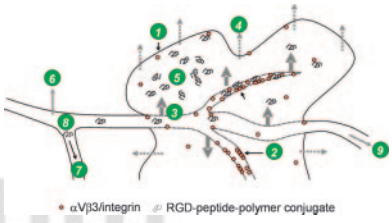

Boecker and colleagues quantify the binding kinetics of the novel PET tracer ^{18}F-FDPN for opiodergic system imaging and assess the effects of scanning duration in an effort to determine an optimal protocol. . . . . ***Page 2092***

Ginj and colleagues report on the design, synthesis, and preclinical assessment of new trifunctional conjugates of somatostatin that target the nucleus to provide a better carrier for Auger electron–emitting radionuclides and ensure longer retention in tumor cells. . . . . ***Page 2097***

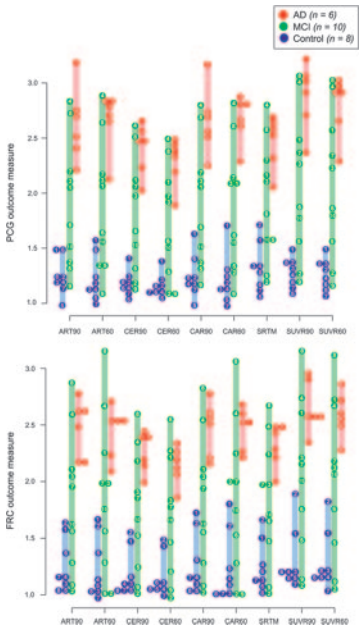

Kersemans and colleagues describe and evaluate the tumor-detecting characteristics and kinetics of $^{123/125}$I-2-iodo-D-phenylalanine, a radiolabeled amino acid analog with promise in diagnostic imaging. . . . . ***Page 2104***

Brogsitter and colleagues investigate whether intraarterial application of ^{131}I-MIBG has the potential to enhance tumor uptake in a population of patients with primary or metastasized neuroendocrine tumors. . . . . ***Page 2112***

ON THE COVER

The newly developed ^{18}F-FLT PET is compared with the routinely used ^{11}C-MET PET and contrast-enhanced MRI in these images of a 26-y-old woman with a WHO grade I astrocytoma. The findings illustrate the ability of ^{18}F-FLT PET to determine DNA metabolism and amino acid uptake, as well as the integrity of the blood–brain barrier, in patients with gliomas and clarify the role of ^{18}F-FLT in the diagnosis of primary central nervous system tumors.